Aerosol Science and Technology

ISSN: (Print) (Online) Journal homepage: www.tandfonline.com/journals/uast20

Microfluidic enabled ice nucleation studies of montmorillonite clay at varying pH and ionic strengths with refreezing and relative humidity cycling

Margaret L. House & Cari S. Dutcher

To cite this article: Margaret L. House & Cari S. Dutcher (17 Jul 2024): Microfluidic enabled ice nucleation studies of montmorillonite clay at varying pH and ionic strengths with refreezing and relative humidity cycling, Aerosol Science and Technology, DOI: 10.1080/02786826.2024.2371412

To link to this article: https://doi.org/10.1080/02786826.2024.2371412

AEROSOL SCIENCE AND TECHNOLOGY
https://doi.org/10.1080/02786826.2024.2371412

Microfluidic enabled ice nucleation studies of montmorillonite clay at varying pH and ionic strengths with refreezing and relative humidity cycling

Margaret L. House[a] and Cari S. Dutcher[a,b]

[a]Chemical Engineering and Materials Science, University of Minnesota Twin Cities, Minneapolis, Minnesota, USA; [b]Mechanical Engineering, University of Minnesota Twin Cities, Minneapolis, Minnesota, USA

ABSTRACT

Atmospheric aerosol particles can impact the optical depth of mixed-phase clouds through heterogeneous ice nucleation. Ice nucleating particles (INP) are therefore important contributors to global and local climate but remain under-parameterized in climate models, partially due to the complex interaction between composition and processing conditions. In this article, we study the ice nucleation (IN) activity of montmorillonite bentonite clay which is a common model dust INP, utilizing a 150-well microfluidic device. Refreezing tests are carried out for solutions across a range of salinity and pH to determine the impact of composition and processing on droplet freezing behavior, with and without an intermediate relative humidity (RH) cycling step. It is found that freezing order deviation dramatically increases after droplets undergo RH cycling, and the potential influence on IN activity of delamination of clay when subjected to changing RH conditions is discussed. Freezing order deviation decreases with increasing solution ionic strength, a trend linked to the delamination behavior of bentonite clays, and an overall decrease in IN activity at low pH is observed, possibly due in part to pH-dependent changes in clay aggregate size distribution. The authors conclude that pH changes and RH processing, such as those which naturally occur in the atmosphere, have a marked impact on the IN activity of clay-containing aerosol droplets.

GRAPHICAL ABSTRACT

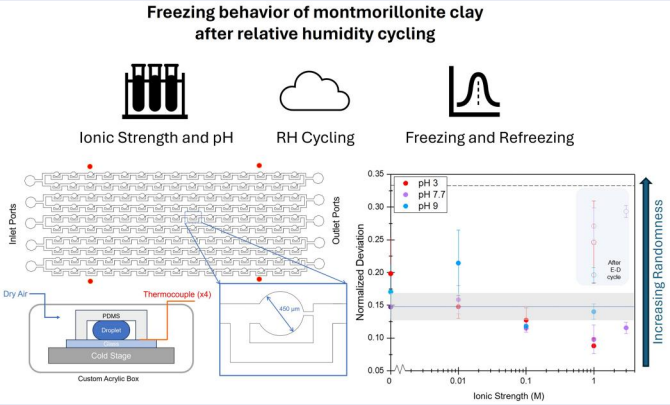

ARTICLE HISTORY
Received 8 March 2024
Accepted 28 May 2024

EDITOR
Nicole Riemer

Introduction

A full picture of aerosol impacts on key atmospheric processes such as gas-particle partitioning, water uptake, and phase transformation remains a challenge to complete, partially due to the physical and chemical complexity of individual aerosol droplets and particles. Atmospheric aerosols range in size from nanometers to tens of microns (Boucher 2015), and can contain soot, dusts, inorganic salts and acids, organic acids and other organic components, bacteria, and other biological components like pollen, fungi, and viruses (Burrows et al. 2022; Hoose and Möhler 2012). Chemical reactions occur within and on the surface of these aerosol particles, and physical aging further

CONTACT Cari S. Dutcher cdutcher@umn.edu Mechanical Engineering, University of Minnesota Twin Cities, 111 Church St., Minneapolis, MN 55455, USA.

Supplemental data for this article can be accessed online at https://doi.org/10.1080/02786826.2024.2371412.

changes the chemical and physical properties over time. The combined chemical and physical properties across an aerosol population are defined as the physicochemical mixing state (Ault and Axson 2017; Riemer et al. 2019), an analog to the better-understood chemical mixing state defined as the distribution of chemical species across the individual particles with in an aerosol population.

Physicochemical mixing state impacts the ice nucleating (IN) activity of individual aerosol particles. Particles which nucleate ice in a cloud are referred to as ice nucleating particles (INP). The presence of INP in clouds changes the overall albedo of the clouds by freezing all or part of the cloud, leading to greater optical extinction through the cloud which may cool the surface underneath (Vergara-Temprado et al. 2018). Partially frozen clouds, commonly referred to as mixed-phase clouds, are a main cause of increased optical depth in clouds, which is represented across several global climate models (GCMs) (Bellouin et al. 2020). However, incomplete characterization of INP concentrations and ice formation microphysics limits the accuracy of GCMs in predicting the magnitude of change in mixed phase cloud albedo, as well as the sensitivity of albedo to global and local warming (Bellouin et al. 2020; Ceppi et al. 2017). Further research into the microphysical IN activity of individual cloud droplets is needed to increase the predictive power of GCMs, for which further research into the microphysical IN activity of individual droplets is urgently needed.

Single particle measurement techniques can elucidate microphysical INP properties by probing the freezing behavior of particles of varying composition, shape, size, and location of origin in both online and off-line configurations. Microfluidic platforms are emerging in the field of atmospheric aerosol science and are a useful complementary approach to more traditional single droplet work, due to their low cost, ease of manufacturing, and small aerosol sample size requirements. A review of current microfluidic methods for studying single droplets, including those of atmospheric relevance, has been given by Roy, Liu, and Dutcher in Annual Reviews of Physical Chemistry, 2021. Broadly, microfluidic ice nucleation methods fall into two categories: flow-through and static. Recent examples of flow-through devices include those used by the Murray group (Tarn et al. 2021) and the Dutcher group (Roy, House, et al. 2021). Examples of static devices for ice nucleation include the WISDOM (Eickhoff et al. 2023; Reicher, Segev, and Rudich 2018), the MINCZ (Isenrich et al. 2022), and the static well arrays used by the Sullivan group (Brubaker et al. 2020) and the Dutcher group (House and Dutcher 2023; Roy, House, et al. 2021). Temperature gradient control in flow-through microfluidics has seen recent progress using Peltier coolers (Liu et al. 2023; Roy, House, et al. 2021), but cooling rate remains easiest to control using static droplet devices, especially for achieving the low cooling rates typical in clouds (Klinger, Feingold, and Yamaguchi 2019).

In addition to ice nucleation behavior in a single freezing cycle, refreezing of particles is of atmospheric interest. Particles that act as ice nuclei in the atmosphere may do so over several freezing and thawing cycles. A change in IN efficiency after freezing may contribute to observed atmospheric phenomena in deposition freezing mode such as the total glaciation of clouds above volcanic ash plumes (Marcolli 2017), continuous ice nucleation in long-lived mixed phase clouds (Fridlind et al. 2012; Jing et al. 2022), and 'natural cloud seeding' which is the nucleation of ice within clouds by falling ice that has sedimented out of a cloud above them (Proske et al. 2021). Unique refreezing behavior has also been noted in surfactant systems related to marine aerosols (Perkins et al. 2020), where higher IN activity upon refreezing was theorized to occur due to the surfactant monolayers changing shape to accommodate growing ice crystals, as well as in biological INP systems (House and Dutcher 2023).

Along with the temperature cycling that can affect INP, atmospheric aerosols undergo relative humidity (RH) cycling throughout each day (Yao et al. 2021). Relative humidity cycling is part of typical 'cloud processing' experiments, in which particles are subjected to several cloud growth and evaporation cycles (Bertozzi et al. 2021; Schuster, Lin, and Dubovik 2009). Cloud processing has been shown to enhance ice nucleation in soot particles mixed with sulfate and organics (Gao and Kanji 2022), as well as in particles of secondary organic aerosol (Wagner et al. 2017) in deposition freezing, although such results cannot be used to predict immersion freezing behavior (Holden et al. 2021). Cloud processing including RH cycling may increase the chemical reactivity of mineral dusts such as clays (Matsuki et al. 2010; Wang et al. 2019), but little is currently known about the effect of RH cycling on clay IN efficiency.

Montmorillonite clay, a common clay found in soils and atmospheric aerosols, is a composite of many sheets of aluminosilicate bound by charge. Its morphology is highly sensitive to cation size and

concentration (Ahmed et al. 2016). Wilkinson et al. studied the impact of ionic strength on morphology of bentonite clay aggregates, noting different size distributions at increasing ionic strengths (Wilkinson et al. 2017). Due to the high prevalence of marine aerosols in the marine boundary layer of the atmosphere (Quinn et al. 2023), dusts/clays and salt are often found in the same aerosol droplet (Adachi et al. 2022) and can be found in ice residuals from mixed phase clouds (Eriksen Hammer et al. 2018), making clay and NaCl a system with atmospheric IN relevance. A range of solution pH values relevant to marine aerosols (Keene et al. 1998) and prior work with montmorillonite clay (Wilkinson et al. 2018) were also studied. Montmorillonite clay, like all bentonite clays, is morphologically sensitive to pH due to its highly charged edges.

Overall, the goal of the article is to utilize a state-of-the-art microfluidic well array to delve into the IN ability of this common INP under a range of ionic strength and pH values while also exploring the impact of RH cycling on freezing. In order to capture an atmospherically relevant range of pH and ionic interactions with the clay, sodium chloride (NaCl), HCl, and NaOH were added to the aqueous suspensions of montmorillonite clay. We seek to expand on the body of work addressing ice nucleation and refreezing utilizing a microfluidic static well droplet trap device. On this microscale platform, the same droplets can be frozen in multiple cycles, including after they have been subjected to RH cycling. This allows for calculating of an overall freezing spectrum, as well as for observing changes in the order in which the same droplets freeze from test to test. To our knowledge, no other study yet exists on droplet refreezing order and/or RH cycling for immersion freezing experiments of clay INP.

Methods

A detailed description of the static well array device used for these experiments is given in House and Dutcher (House and Dutcher 2023). Briefly, a 150-well array of wells with a diameter of 450 µm (top view in Figure 1a) and a thickness of 143 µm (side view in Figure 1b) is patterned onto a silicon wafer using standard photolithography techniques, with a single well illustrated in Figure 1c. This silicon wafer is silanated to prevent sticking and is used as the device mold. When polydimethylsiloxane (PDMS) rubber is poured over the mold and baked at 70 °C for 24 h, the raised channel and well patterns are cured into the rubber, which can then be peeled off the mold and affixed to a PDMS-coated glass backing slide. The mold can then be reused.

To perform a test, all channels are first flushed with filtered silicone oil (Whatman Anotop Filter, 0.02 µm). Then, a syringe with a 1.2 mm needle is used to fill all channels and wells with the sample to be tested. Finally, filtered silicone oil is again injected into each channel so that the excess aqueous sample is cleared from the channels, leaving only the 450 µm diameter 'pancake'-shaped droplets behind. The device is placed on a temperature controlled cold stage (LTS 420 with LNP96 cooling pump, Linkam Scientific) to which an optics grade mirror is affixed with thermal grease (Ceramique 2, Arctic Silver). Several drops of silicone between the mirror and the device ensure good thermal contact between the two while still allowing for light transmittance. Figure 1b shows a simplified illustration of the experimental set-up. Four designated thermocouple slots in the device, designated with red dots in Figure 1a, hold type-K thermocouples (K Type Mini-Connector Thermocouple, HUATO Environment Monitoring System and Equipment) for the measurement of temperature throughout the test using an Omega 8-channel thermocouple reader and Omega software. Thermocouples are calibrated using the melting temperatures of pure hydrocarbons, as detailed in the online supplementary information (SI). The cold stage and device are covered with a custom laser cut acrylic lid, which has a port for the use of dry air as described later in the methods section.

Linkam control software is used to lower the cold stage first to an intermediary temperature between −10 °C and −20 °C, depending on when first freezing is expected. After it is determined that all thermocouples are reading properly at the intermediary temperature, the cell temperature is lowered by 1° C per minute until freezing of all droplets has been observed. The device and droplets are viewed with a reflected light microscope (SZX10, Olympus), and freezing is denoted by the transparent liquid droplet turning a distinctly darker shade due to the refraction of light by the ice crystals. A video of the freezing droplets is recorded using a 1200 × 1600 px monochromatic camera (acA1600-60gm, Basler) attached to the microscope. After all droplets have frozen, the device is warmed to room temperature at a rate of between 3 °C and 5 °C per minute. Once the droplets are thawed completely, the freezing process is then repeated so that the order of droplet freezing compared to the first freezing test can be obtained. After the second freezing test, the device is warmed to

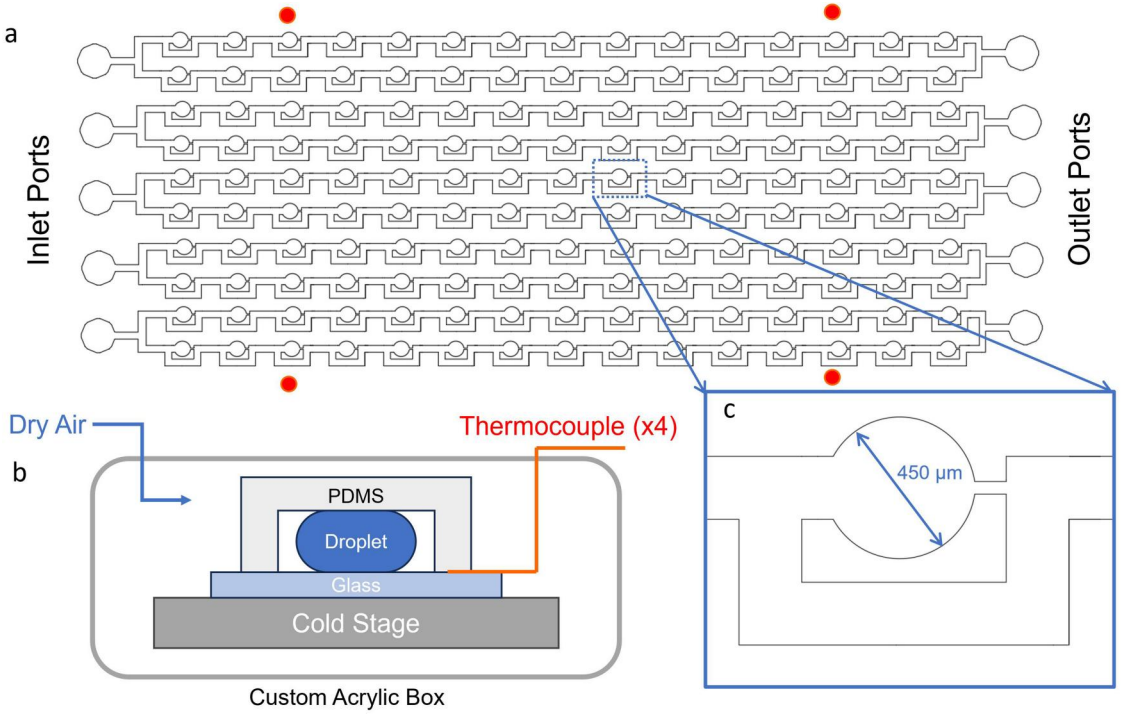

Figure 1. Schematic of (a) the 150 well array mold pattern (top view), (b) a simplified cross-sectional illustration of the experimental setup for one droplet (side view), and (c) an individual static well (top view). Red dots indicate the approximate location of thermocouples. Channel height (thickness) is 143 µm.

room temperature. Throughout all freezing and warming steps, dry air is supplied to the freezing chamber to prevent condensation on the surface of the device and the inner walls of the chamber. On the timescales and at the temperatures of these freezing experiments, little or no pervaporation through the PDMS layer is expected. Condensation still remains a challenge in the humid summer months, leading to reduced available testing time.

Fully thawed devices are placed in a drying chamber at <5% RH. The thermodynamic driving force within the PDMS between the droplets and the dry air causes water molecules to pervaporate from the droplets through the PDMS into the ambient air, leaving behind only clay and NaCl salt as relative humidity is decreased below that where efflorescence occurs. These fully dried droplets are then allowed to reuptake water in a high RH chamber. This efflorescence-deliquescence (E-D) cycle has a marked impact on the IN activity of the droplets and their freezing order, as discussed in the Results section.

Aqueous samples were prepared using Milli-Q water (Millipore Sigma). The water was filtered with a 0.02 µm PTFE Whatman Anotop filter before mixing with HCl, NaOH, clay and/or salts to minimize impurities from the background water. Montmorillinite bentonite clay (Millipore Sigma) was mixed into the water at a concentration of 300 mg/L. No surface treatment is listed for this brand of clay, but milling or cation exchange methods used to optimize the clay for catalysis cannot be ruled out. Montmorillonite clay contains aluminosilicate sheets layered with sodium and calcium cations, with trace amounts of potassium and magnesium cations (Behnsen and Faulkner 2013). It should be noted that the ionic strength values reported here do not account for any contributions from the Montmorillonite clay. Next, the pH of the clay-water mixture, which was 7.7 without adjustment, was adjusted to make aliquots of pH 3 and pH 9 using filtered HCl (Fisher Scientific) and NaOH (Fisher Scientific), respectively; amounts are shown in online SI Tables S2 and S3.

Finally, after ~30 min of mixing the clay with the water post-pH adjustment to ensure a good suspension, NaCl (Fisher Scientific) was added to achieve different ionic strengths; amounts are shown in online SI Tables S4–S6. All aqueous clay-salt solutions were stored in a freezer at −4 °C until the time of testing to prevent microbial growth in the solutions, which could affect IN values.

For particle size distribution measurement of the clay suspensions, a laser diffraction particle size analyzer (LD-PSA, Microtrac Bluewave) was used. Fresh clay-salt mixture was poured into the sample collection slot after 9 rinse cycles with Milli-Q water to ensure a clean background. About 25 mL of clay-salt

solution was required for sufficient signal strength. A preset Bentonite Clay SOP in the Bluewave software was used to measure the size distribution of particles at five different concentrations of NaCl, with an additional eight rinse cycles in between each salt concentration. Volume size distribution is measured, with diameter given assuming spherical particles.

Freezing point depression

The freezing point depression of the NaCl and montmorillonite clay mixtures, ΔT_f, was calculated using Blagden's Law for ideal dilute solutions, given by Equation (1),

$$\Delta T_f \approx iK_f m \tag{1}$$

where i is the van't Hoff factor, or the number of ions per molecule of solute, K_f is the cryoscopic constant of the solvent, and m is the molality of the solution. Using Blagden's Law, the freezing point depression is approximately −3.72 °C for 1 M total ionic strength, since NaCl, HCl, and NaOH all have 2 ions per molecule. The temperatures reported in this article for ionic strength 0.01–1 M are adjusted by the values obtained using Blagden's Law, which accurately captures freezing point depression in our independent tests of pure salt-water solutions. For 3 M ionic strength, the dilute assumption underlying Blagden's Law breaks down, so the freezing point depression correction was determined experimentally. Data for 3 M NaCl empirical freezing point can be found in SI Section 3. It should be noted that Blagden's law approximates the change in the equilibrium melting temperature, whereas the empirical data collected for use in this study measures the change in nucleation temperature between pure water and a solution of 3 M NaCl. At the more dilute concentrations, we assume that nucleation temperature depression and freezing point depression are the same.

Results

Ice nucleation

To make useful comparisons between data collected from our freezing experiments and other immersion freezing experiments, and between our data and data for other atmospheric ice nucleators, we calculate the ice nucleating active site density, or the number of ice nucleating active sites per milligram of clay material, abbreviated as η_m. As a precursor to calculating η_m, the fraction of droplets frozen in the device, called fraction frozen or f(T), is first calculated as a function of temperature, as shown in Equation (2).

$$f(T) = \frac{N_f}{N} \tag{2}$$

where N_f is the number of frozen droplets at a given temperature T, and N is the total number of droplets visible in the viewing window. Temperature from the four thermocouples is averaged across the device. Once frozen fraction as a function of temperature is calculated, η_m can be modeled as a time-independent function of temperature, as shown in Equation (3) (Vali 1971).

$$\eta_m(T) = -\frac{\ln\left(1 - f(T)\right)}{V \times C_m} \tag{3}$$

where η_m is ice nucleating active site density (INAS/mg), V is droplet volume, and C_m is the concentration of nucleating material in the bulk solution, in this case bentonite clay. Since droplets in the microfluidic device are a disc-like, 'pancake' shape, volume is approximated as a cylinder with the border of a taurus, as shown in Equation (4) (Nandy and Dutcher 2018; Vuong and Anna 2012),

$$V = \frac{\pi h^3}{6} + \frac{\pi h}{4}\left(D_{drop} - h\right)\left(\frac{\pi h}{2} + D_{drop} - h\right) \tag{4}$$

where h is the channel height and D_{drop} is the diameter of the droplet.

Figure 2 shows frozen fraction and ice nucleating active site density for three different pH and five different ionic strength values. The concentrations shown are that of total ionic strength with both the NaCl and pH adjustment. 3 M NaCl was only tested on the pH 7.7 mixture, as the high molarity led to extreme freezing point depression and thus high levels of condensation during the tests, which was exacerbated at pH 3. A background of pure, pH neutral water (black crosses) is also reported for comparison. In the plots above, INAS density is reported in sites per milligram of clay. However, to compare our values to those seen in existing literature on the IN efficiency of montmorillonite clay, INAS/mg was also converted to INAS/m^2 using the BET surface area of bentonite clays. This value has been reported as falling between 50 and 130 m^2/g for unprocessed montmorillonite clays (Kaufhold et al. 2010), so a median value of 90 m2/g was chosen. When vertical error bars are added to represent INAS/m^2 assuming the lowest and highest

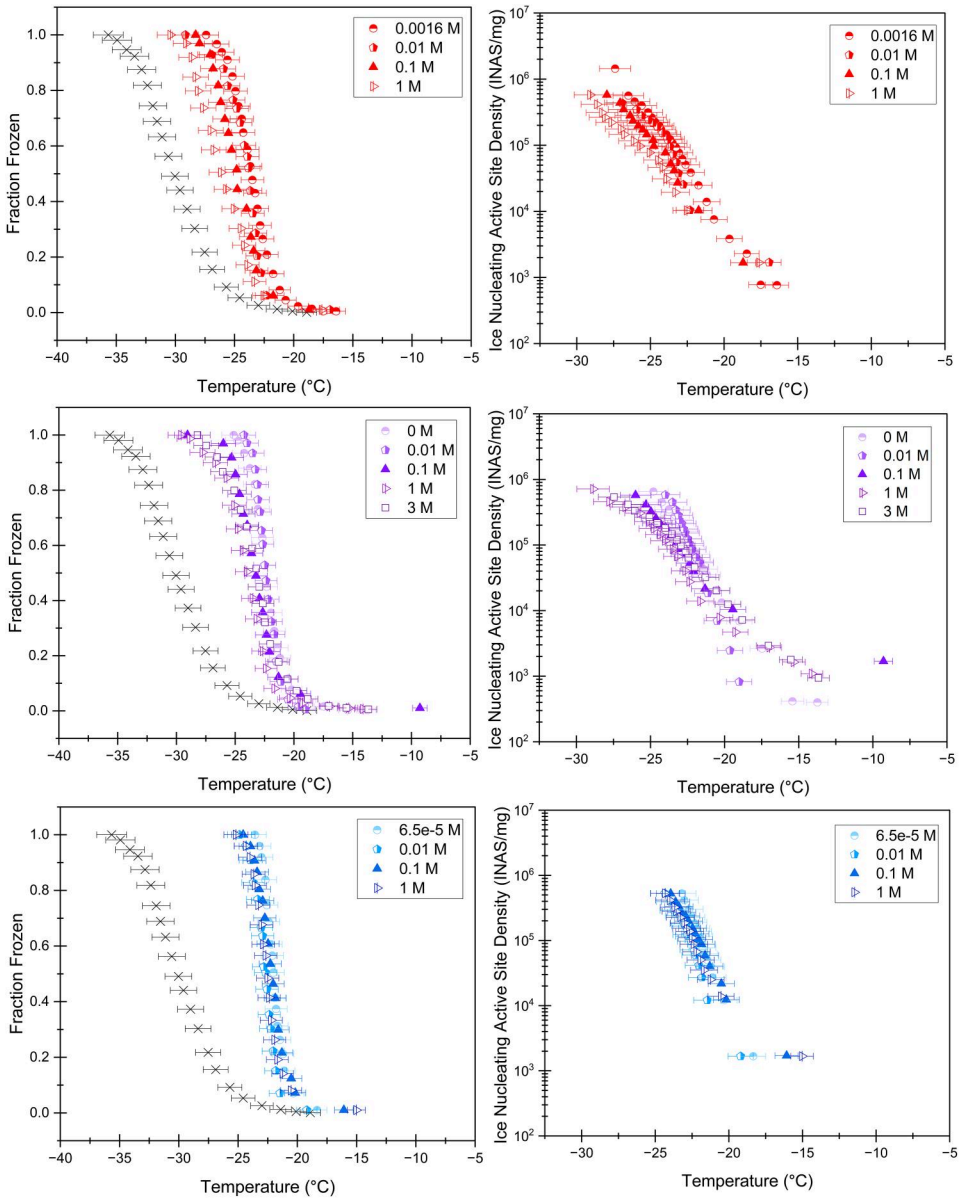

Figure 2. Frozen fraction versus temperature and INAS versus temperature curves for pH 3 (red), pH 7.7 (purple), and pH 9 (blue) mixtures of 300 mg/L montmorillonite clay and NaCl, with total ionic strength from the added salts labeled. HCl and NaOH are used for pH adjustment (concentrations given in SI section S2). Black crosses indicate background freezing of Milli-Q water. All curves are corrected for freezing point depression based on total ionic strength, and background INAS is not subtracted from reported INAS values. For more information on error bar calculation, refer to Section 1 of the online supplementary information.

BET surface areas, the error bars are so small that they are hidden behind the graphical symbols and so are omitted for clarity. Figure 3 shows the results of the non-pH adjusted bentonite clay in this work compared to the INAS/m^2 of several other articles.

The reported ice nucleating active site density from this work shows best agreement with the values from Pinti et al. (2012) and Attard et al. (2012), though it should be noted that variations in these clay systems are expected depending on source. The pH of the clay solution used for our data points was 7.7. The pH of the solutions in the articles cited in Figure 3 were not provided. All studies shown in Figure 3 were carried out in the immersion mode, but deposition freezing on montmorillonite clay is another experimental setup that can produce INAS density values within this range (Welti et al. 2009; Zimmermann et al. 2008).

Figure 4 compares the three different solution pH values directly to each other at four ionic strength values. Again, the concentrations shown are that of total ionic strength with both the NaCl and pH adjustment. Even after freezing point depression adjustment, increasing ionic strength appears to decrease IN activity most strongly for pH 3 solutions, with a weaker

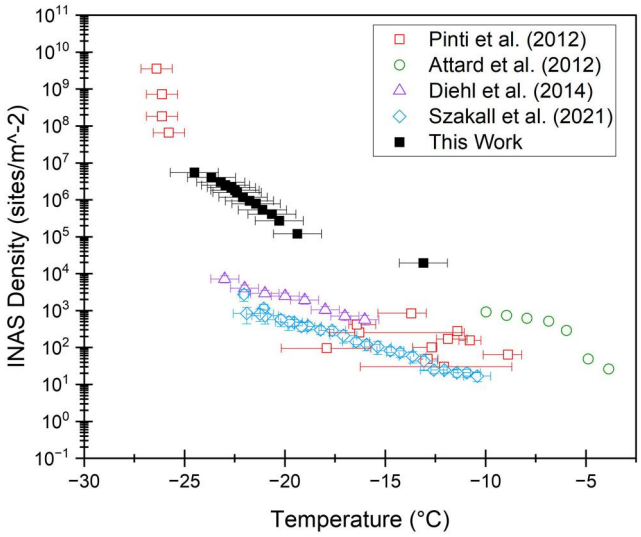

Figure 3. Ice nucleating active site (INAS) density normalized by ice nucleator BET surface area, with values from this work at pH 7.7 and no additional salt and reported results from several articles studying immersion freezing (Attard et al. 2012; Diehl et al. 2014; Pinti et al. 2012; Szakáll et al. 2021). For the first two referenced works, the calculations in the review by Hoose and Mohler were used for INAS density (Hoose and Möhler 2012). Error bars for literature values are provided where available. For more information on error bar calculation for the data from this work, refer to Section 1 of the online supplementary information. Note that all studies are for immersion freezing, and that values for Pinti et al. 2012 comprise bulk and emulsion freezing. Additionally, montmorillonite clay type (i.e., cation and processing conditions) differs between and within studies.

effect on pH 7.7 solutions, as seen in Figures 2 and 4. At each ionic strength, clay mixtures adjusted to pH 3 show less efficient ice nucleation than pH 7.7 (no adjustment) or pH 9. In both Figures 2 and 4, the background freezing curve for water is higher than purely homogeneous freezing for droplets of this volume. This is due to the presence of some impurities in the background water as well as imperfections in the devices leading to ice nucleation sites.

Refreezing and E-D cycling

Samples at all pH values and ionic strengths were subjected to refreezing tests, as well as E-D cycling, to determine their impact on IN activity. The experimental metric recorded for determining relative stochasticity of clay freezing was freezing order, or the order in which each well froze in each test. In a fully deterministic 'ideal' ice nucleation experiment, the order in which droplets froze would not change from test to test. To quantify this deviation from a fully deterministic test, the 'normalized deviation' was calculated. For each given well 'n' visible in the viewing window, d_n is given by Equation (5)

$$d_n = \frac{(|order_{test\ 1} - order_{test\ 2}|)_n}{N} \quad (5)$$

where $order_{test\ 1,2}$ is the number representing in what order well 'n' froze in test 1 or in test 2. For example, if well 'n' froze 23rd in test 1, $order_{test\ 1}$ would be 23, and if the same well 'n' froze 38th in test two, $order_{test\ 2}$ would be 38. N is the total number of wells in the viewing window. N is the same in test 1 and test 2. In a typical test, N is ~100. No significant change in freezing temperature curves is noted between tests with or without E-D cycling. For more information on freezing curves before and after refreezing and E-D cycling, see SI Section 4.

In Figure 5, average normalized deviation is plotted against ionic strength. Deviation from the ideal case of zero deviation appears to decrease with increasing ionic strength, while dramatically increasing (shaded region labeled 'After E-D cycle') after an efflorescence-deliquescence cycle. To calculate the value of normalized deviation for a device in which freezing order was fully random, simulations in MATLAB assigned random freezing order values for 100 wells over two tests (note, this type of simple simulation does not take into account the Poisson distribution inherent in freezing). The random-order normalized deviation value is 0.33 ± 0.005, which is higher than any normalized deviation value from our experiments. For more information on random-order freezing simulations, see the SI.

The averaged normalized deviation observed in Figure 5 may arise in our microfluidic device through internal (single well) and external (between wells) variability (Deck and Mazzotti 2023; in particular, see their experiments and stochastic simulations in their Figure 6). To explore the type of variability in our experiments, the distribution of freezing temperatures by well between Freezing Test 1 and Freezing Test 2 is shown in the SI (Figure S5), for the 0 M, pH3 case which showed the highest normalized deviation value. Roughly half (44%) of wells show freezing temperature variability outside of the error bars of the device, particularly those that froze at lower temperatures. The results suggest that our data lies somewhere between stochastic and deterministic freezing behavior.

Discussion

From the results, three overall trends emerge: (1) Mixtures of 300 mg/L montmorillonite clay adjusted

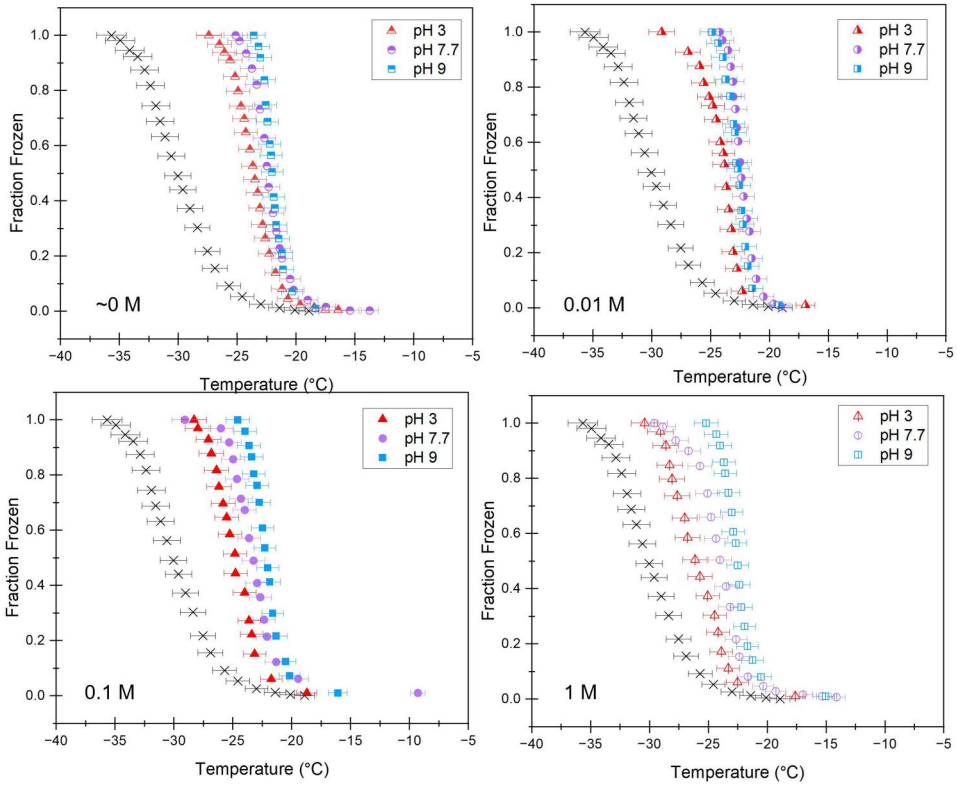

Figure 4. Frozen fraction versus temperature and INAS versus temperature curves for pH 3 (red), pH 7.7 (purple), and pH 9 (blue) mixtures of 300 mg/L montmorillonite clay and NaCl, with total ionic strength labeled on each graph. HCl and NaOH are used for pH adjustment (concentrations given in SI section S2). All data shown are the same as in Figure 2, reordered for clarity. For the 0 M (top left) plot, pH 3 actual ionic strength from the added salt to adjust the pH is 0.0016 M, and pH 9 actual ionic strength is 6.5e-5 M. Black crosses indicate background freezing. All curves are corrected for freezing point depression based on total ionic strength. For more information on error bar calculation, refer to Section 1 of the online supplementary information.

to pH3 with HCl are consistently less IN active than their counterparts at pH 7.7 and pH 9, (2) Freezing order normalized deviation decreases (i.e., demonstrates more deterministic freezing behavior) with increasing ionic strength, and (3) Freezing order normalized deviation dramatically increases after E-D cycling. This discussion section links clay aggregate size dispersity with IN activity for solutions at pH 3 and pH 7.7. The RH-independent component of refreezing order observed in these experiments is compared with results obtained in other clay IN preactivation studies. Finally, the role of clay aggregate delamination is examined and linked to E-D cycled refreezing order.

Aggregate size and ice nucleation activity

pH 3 Clay mixtures are consistently less IN active than their counterparts at pH 7.7 and pH 9, across varying ionic strengths. Literature on clay subjected to highly acidic solutions shows that acid processing decreases clay IN activity, potentially by changing the structure of montmorillonite clay from hexagonal to monocyclic (Sihvonen et al. 2014). However, this acid processing is done at high acidic concentrations with strong acids such as sulfuric or nitric acid, conditions which are not met in our mildly acidic pH 3 solution. To investigate potential causes of the decrease in IN activity, the changes in volume size distribution of pH 3 and pH 7.7 particles due to changes in clay aggregation were measured using laser diffraction, as described in the methods section.

Figure 6 shows the percentage of the total sample versus each diameter bin for pH 3, pH 7.7, and pH 9 systems at different NaCl concentrations. At low pH, there is significantly less size polydispersity in the clay mixtures, a trend also observed by Wilkinson et al. in clay mixtures ranging from pH 3 to pH 11 (Wilkinson et al. 2018), although exact sizes observed are different due to differences in concentrations between the two studies. Welti et al. found that in deposition freezing studies on montmorillonite and kaolinite, larger particles were more efficient ice nucleators, although due to the nature of the tests the freezing temperatures sampled were much lower than those in this article (Welti et al. 2009). In immersion

freezing measurements at the Leipzig Aerosol Cloud Interaction Simulator, kaolinite particles with diameters 300, 500, and 1000 nm were found to have similar INAS densities; this led to freezing probability increasing exponentially with surface area. Particle sizes in this study by Hartmann et al. were much lower than the bulk of clay particulates in this article, and the associated freezing temperatures were lower (Hartmann et al. 2016). Surface area is an important contributor to IN activity for immersion freezing even at much larger particle sizes.

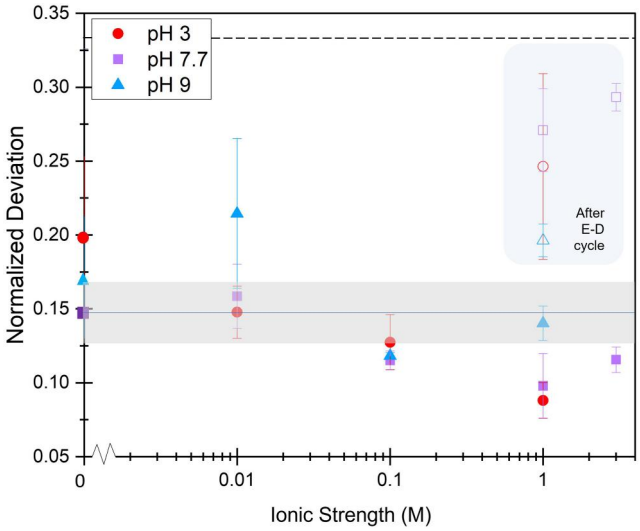

Figure 5. Averaged normalized deviation versus ionic strength for pH 3 (red), pH 7.7 (purple) and pH 9 (blue) mixtures of 300 mg/L bentonite montmorillonite clay and NaCl, with small amounts of HCl and NaOH are used for pH adjustment. Ionic strength is total solution ionic strength from the added salts. Closed symbols indicate refreezing with no cycling between tests, while open symbols denote refreezing with an E-D cycle between tests. The blue shaded region is added for further clarity in denoting tests that have an intermediate E-D cycle. Horizontal blue line indicates the normalized deviation for pure water in our system, with the grey box denoting the error bars of pure water at ionic strength 0 M; normalized deviation was not collected for pure water at other ionic strengths and could differ from the value shown. The dashed black line indicates the result for normalized deviation of 100 simulations for a freezing system where well freezing order is randomly generated. Error bars for the simulation value are <0.005. For more information on the simulations, see the online supplementary information.

Based on the results from the laser diffraction measurements in Figure 6, and assuming a spherical shape for each size bin, the pH 3 solutions have more available surface area than the pH 7.7 and pH 9 solutions at ionic strengths below 1 M. This appears to be at odds with the decreased IN capability of ph3 solutions; there is more available surface area in a droplet of pH 3 solution, but lower IN capability. This points to an IN behavior dominated by ice active sites that are not evenly distributed across spherical surface area. Since the volume distribution is measured by laser diffraction, radius is estimated based on the assumption of spherical particles. However, clay particles are often irregular and non-spherical, which may lead to inaccuracies in the particle size estimation by laser diffractometry. Additionally, as the sign of the edge charges changes from positive at pH 3, to neutral at pH 6.5, to negative at pH 7.5 (Kumar et al. 2023), the edge charges could be influencing IN capability. These edges would not be differentiated from the bulk using laser diffraction. At 1 M ionic strength, available surface area for pH 7.7 and 9 mixtures increases dramatically but remains lower than available surface area for pH 3 mixture.

The role of delamination and E-D cycling

Swelling and delamination in aluminosilicate clay systems influence the size, shape, and IN ability of the resulting clay aggregates in solution. As shown in Figure 7a and b, montmorillonite clay, like other smectites, exists as flat, thin layers with edges whose

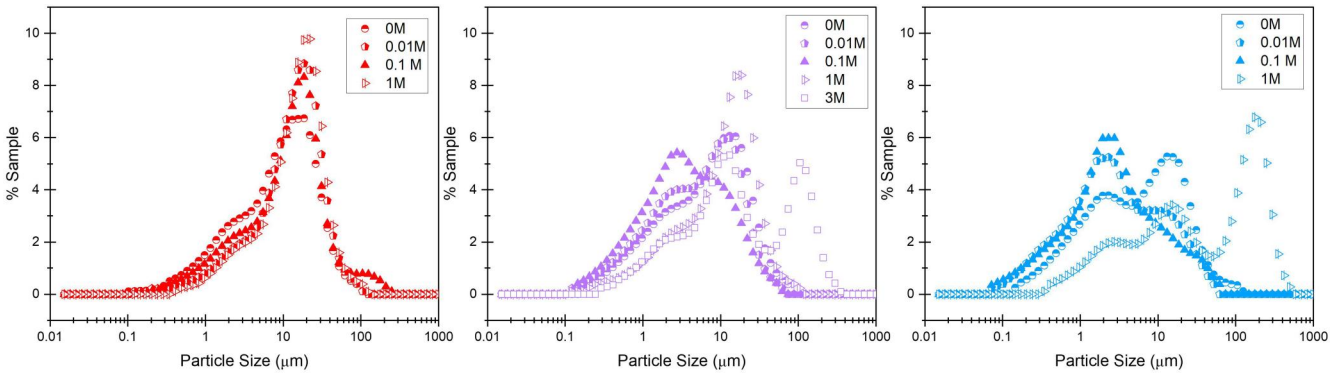

Figure 6. Volume size distribution of particles in 300 mg/L solutions of montmorillonite clay and NaCl at pH 3 (red), pH 7.7 (purple), and pH 9 (blue). Denoted concentrations are of total ionic strength from the added salts.

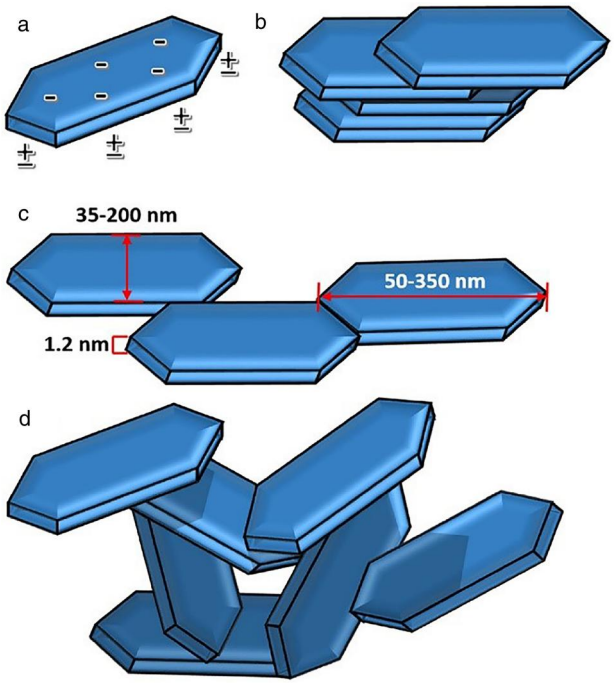

Figure 7. Schematic of bentonite clay sheets (Wilkinson et al. 2017). Reprinted from Colloids and Surfaces A: Physicochemical and Engineering Aspects, 529, Wilkinson, N., A. Metaxas, E. Brichetto, S. Wickramaratne, T. M. Reineke, C. S. Dutcher. "Ionic strength dependence of aggregate size and morphology on polymer-clay flocculation" 1037-1046 © 2017 Elsevier B.V. with permission from Elsevier.

charge is sensitive to pH and ionic strength (Kumar et al. 2023). The layers stack together, bound by charge, and the resulting aggregates contain about 20 clay sheets on average (Cases et al. 1992). When mixed into water, the aggregates swell with water in between the layers, and then the layers separate into clusters <10 layers thick (Segad et al. 2012). Under certain ionic conditions, full delamination can occur. The timescale of swelling and delamination occurs on the order of minutes to months, depending on the exchangeable cations present in the solution and the initial size of the clay aggregates (Kumar et al. 2023). Once the particles are partially or fully delaminated, the highly charged edges can interact with the faces of the sheets to form new, larger porous clusters as shown in Figure 7c and d, and, over time, even complex structures like gels (Pujala and Bohidar 2019; Suman and Joshi 2018).

The edges of the hydrated clay clusters, being highly hydroxylated and pH sensitive, are the most likely candidates for ice nucleation active sites (Kumar et al. 2023). The ideal size of clay aggregate for ice nucleation of water is three layers thick or larger, since the thickness of a single clay sheet, ~1 nm (Nicola, Bernardo-Gusmão, and Schwanke 2021), is too small to facilitate freezing (Kumar et al. 2023). Therefore, for peak IN efficiency, swelling or partial delamination is desirable. Highly saline solutions do not allow for complete delamination of clay particles, and inhibit swelling (Ahmed et al. 2016). This may explain the bimodal particle distribution and large particles observed in the 3 M NaCl clay mixture. More studies with different cations are warranted to probe this phenomenon further. After E-D cycling, the deviation from deterministic behavior is much more pronounced. This may be due to a second swelling and delamination process occurring as the dried clay re-uptakes water. This could change the stacking and agglomeration of clay sheets in the droplets as compared to the first freezing test, exposing differing edge morphologies which are the dominant source of IN sites (Freedman 2015; Klumpp et al. 2023; Kumar et al. 2023; Kumar, Marcolli, and Peter 2019).

Refreezing behavior without E-D cycling

In our measurements, no significant change was observed in IN temperature between freezing tests. However, the normalized deviation of freezing order between tests, higher than the deterministic limit of 0 but lower than the random limit of 0.33, suggests that freezing may change the structure or number of ice nucleation sites available on the clay particles.

Several articles have referenced a 'pre-activation' behavior for clay INP (Jing et al. 2022; Marcolli 2017). Pre-frozen, or pre-activated, clay particles appear to re-freeze at warmer temperatures. The range of temperature change depends on the material, the temperature the frozen particles are held at, and other factors. However, these tests are carried out at well below the melting point of water, and utilize deposition nucleation in the clay nano-pores (Marcolli 2017). Our immersion freezing tests include a complete thawing of all droplets and subsequent warming to room temperature. The edges of aluminosilicate clays are the dominant source of IN active sites (Freedman 2015). For our immersion freezing set up, changes in the layer stacking leading to differing edge morphology are the most likely source of changes in IN activity between freezing and thawing cycles, although the exact mechanism by which this change in edge availability would occur in our experimental setup is not immediately clear.

Conclusion

Montmorillonite clay solutions at a range of pH and ionic strengths were tested for their IN ability using a

150-well microfluidic device to determine the influence of refreezing and E-D cycling on ice nucleation activity. For the non-pH adjusted clay solutions, results for area normalized INAS density as a function of temperature showed agreement with several other studies. Overall, a wide range of reported INAS densities for montmorillonite clay exist in literature, showing the complexity of even this simple model atmospheric aerosol system. In this work, it was found that at pH 3, clay solutions nucleate ice less efficiently than at higher pH values. For ionic strengths below 1 M, the total available surface area is increased for pH 3 particles using laser diffraction measurements of volume size distribution assuming spherical particles, compared to that from pH 7.7 and pH 9. The fact that higher available surface area does not correspond to higher IN activity suggests a nonuniform distribution of INAS density over the surface of the clay particles. The pH sensitive edges may contribute to IN activity without being discernible from the bulk in laser diffraction measurements. The acidity of the solution may fundamentally change surface properties of the particulates, lowering their IN efficiency (Sihvonen et al. 2018).

Refreezing tests were performed with and without E-D cycling. 'Normalized deviation' was defined as a quantitative measurement of deviation from deterministic behavior, where higher values of normalized deviation denote a more randomized order of freezing. Without E-D cycling, normalized deviation decreased with increasing salinity. With E-D cycling, normalized deviation drastically increased compared to refreezing without E-D cycling. This may be due to delamination in the clay particulates after E-D cycling, though more research is warranted into the phenomena of E-D cycling and how it impacts clay particulates size and structure. Future tests may include more refreezing cycles, as more cycles would provide more robust statistics, although challenges such as condensation must be overcome with more times one device spends at low temperature. As an additional note, more pH values should be reported for immersion freezing experiments of dusts and clays, especially those of pure clay samples for modeling aerosol parameters. pH is an important contributor to size distribution and surface chemistry of montmorillonite clays and other smectites. pH can ultimately influence atmospheric processes like ice nucleation, which impact global temperature and climate and must be correctly represented in global climate models which base their INP parameters on benchtop experiments.

Acknowledgments

The authors thank collaborators from NSF CAICE and Dutcher group member Iaroslav Makhnenko for device fabrication assistance. The authors also thank and acknowledge undergraduate researcher Keiona Williams for contributing to the 3M NaCl freezing measurements. Special thanks is also given to UMN Ph.D. candidate Parth Bhide for assistance in image processing software.

Disclosure statement

No potential conflict of interest was reported by the author(s).

Funding

This work was supported by NSF through the NSF Center for Aerosol Impacts on Chemistry of the Environment (CAICE), an NSF Funded Center for Chemical Innovation (CHE-1801971). Portions of this work were conducted in the Minnesota Nano Center, which is supported by the National Science Foundation through the National Nanotechnology Coordinated Infrastructure (NNCI) under Award Number ECCS-2025124. Any opinions, findings, and conclusions or recommendations expressed in this material are those of the authors and do not necessarily reflect the views of the National Science Foundation.

ORCID

Margaret L. House http://orcid.org/0009-0002-7191-3985
Cari S. Dutcher http://orcid.org/0000-0003-4325-9197

References

Adachi, K., Y. Tobo, M. Koike, G. Freitas, P. Zieger, and R. Krejci. 2022. Composition and mixing state of arctic aerosol and cloud residual particles from long-term single-particle observations at zeppelin observatory, svalbard. *Atmos. Chem. Phys.* 22 (21):14421–39. doi: 10.5194/acp-22-14421-2022.

Ahmed, A. A., I. M. Saaid, N. A. M. Akhir, and M. Rashedi. 2016. Influence of various cation valence, salinity, ph and temperature on bentonite swelling behaviour 1774. doi: 10.1063/1.4965087.

Attard, E., H. Yang, A.-M. Delort, P. Amato, U. Pöschl, C. Glaux, T. Koop, and C. E. Morris. 2012. Effects of atmospheric conditions on ice nucleation activity of *pseudomonas*. *Atmos. Chem. Phys.* 12 (22):10667–77. doi: 10.5194/acp-12-10667-2012.

Ault, A. P., and J. L. Axson. 2017. Atmospheric aerosol chemistry: Spectroscopic and microscopic advances. *Anal. Chem.* 89 (1):430–52. doi: 10.1021/acs.analchem.6b04670.

Behnsen, J., and D. R. Faulkner. 2013. Permeability and frictional strength of cation-exchanged montmorillonite. *JGR. Solid Earth* 118 (6):2788–98. doi: 10.1002/jgrb.50226.

Bellouin, N., J. Quaas, E. Gryspeerdt, S. Kinne, P. Stier, D. Watson-Parris, O. Boucher, K. S. Carslaw, M.

Christensen, A. L. Daniau, et al. 2020. Bounding global aerosol radiative forcing of climate change. *Rev. Geophys.* 58 (1):e2019RG000660. doi: 10.1029/2019rg000660.

Bertozzi, B., R. Wagner, J. Song, K. Höhler, J. Pfeifer, H. Saathoff, T. Leisner, and O. Möhler. 2021. Ice nucleation ability of ammonium sulfate aerosol particles internally mixed with secondary organics. *Atmos. Chem. Phys.* 21 (13):10779–98. doi: 10.5194/acp-21-10779-2021.

Boucher, O. 2015. *Atmospheric aerosols: Properties and climate impacts*. Dordrecht: Springer Nature.

Brubaker, T., M. Polen, P. Cheng, V. Ekambaram, J. Somers, S. L. Anna, and R. C. Sullivan. 2020. Development and characterization of a "store and create" microfluidic device to determine the heterogeneous freezing properties of ice nucleating particles. *Aerosol Sci. Technol.* 54 (1):79–93. doi: 10.1080/02786826.2019.1679349.

Burrows, S. M., C. S. Mccluskey, G. Cornwell, I. Steinke, K. Zhang, B. Zhao, M. Zawadowicz, A. Raman, G. Kulkarni, S. China, et al. 2022. Ice-nucleating particles that impact clouds and climate: Observational and modeling research needs. *Rev. Geophys.* 60 (2). doi: 10.1029/2021RG000745.

Cases, J. M., I. Berend, G. Besson, M. Francois, J. P. Uriot, F. Thomas, and J. E. Poirier. 1992. Mechanism of adsorption and desorption of water vapor by homoionic montmorillonite. 1. The sodium-exchanged form. *Langmuir* 8 (11):2730–9. doi: 10.1021/la00047a025.

Ceppi, P., F. Brient, M. D. Zelinka, and D. L. Hartmann. 2017. Cloud feedback mechanisms and their representation in global climate models. *WIREs Clim. Change* 8 (4): e465. doi: 10.1002/wcc.465.

Deck, L.-T., and M. Mazzotti. 2023. Characterizing and measuring the ice nucleation kinetics of aqueous solutions in vials. *Chem. Eng. Sci.* 272:118531. doi: 10.1016/j.ces.2023.118531.

Diehl, K., M. Debertshäuser, O. Eppers, H. Schmithüsen, S. K. Mitra, and S. Borrmann. 2014. Particle surface area dependence of mineral dust in immersion freezing mode: Investigations with freely suspended drops in an acoustic levitator and a vertical wind tunnel. *Atmos. Chem. Phys.* 14 (22):12343–55. doi: 10.5194/acp-14-12343-2014.

Eickhoff, L., M. Keßler, C. Stubbs, J. Derksen, M. Viefhues, D. Anselmetti, M. I. Gibson, B. Hoge, and T. Koop. 2023. Ice nucleation in aqueous solutions of short- and long-chain poly(vinyl alcohol) studied with a droplet microfluidics setup. *J. Chem. Phys.* 158 (15):154504. doi: 10.1063/5.0136192.

Eriksen Hammer, S., S. Mertes, J. Schneider, M. Ebert, K. Kandler, and S. Weinbruch. 2018. Composition of ice particle residuals in mixed-phase clouds at jungfraujoch (switzerland): Enrichment and depletion of particle groups relative to total aerosol. *Atmos. Chem. Phys.* 18 (19):13987–4003. doi: 10.5194/acp-18-13987-2018.

Freedman, M. A. 2015. Potential sites for ice nucleation on aluminosilicate clay minerals and related materials. *J. Phys. Chem. Lett.* 6 (19):3850–8. doi: 10.1021/acs.jpclett.5b01326.

Fridlind, A. M., B. Van Diedenhoven, A. S. Ackerman, A. Avramov, A. Mrowiec, H. Morrison, P. Zuidema, and M. D. Shupe. 2012. A fire-ace/sheba case study of mixed-phase arctic boundary layer clouds: Entrainment rate limitations on rapid primary ice nucleation processes. *J. Atmos. Sci.* 69 (1):365–89. doi: 10.1175/JAS-D-11-052.1.

Gao, K., and Z. A. Kanji. 2022. Impacts of cloud-processing on ice nucleation of soot particles internally mixed with sulfate and organics. *JGR. Atmos.* 127 (22). doi: 10.1029/2022JD037146.

Hartmann, S., H. Wex, T. Clauss, S. Augustin-Bauditz, D. Niedermeier, M. Rösch, and F. Stratmann. 2016. Immersion freezing of kaolinite: Scaling with particle surface area. *J. Atmos. Sci.* 73 (1):263–78. doi: 10.1175/JAS-D-15-0057.1.

Holden, M. A., J. M. Campbell, F. C. Meldrum, B. J. Murray, and H. K. Christenson. 2021. Active sites for ice nucleation differ depending on nucleation mode. *Proc. Natl. Acad. Sci. USA.* 118 (18):e2022859118. doi: 10.1073/pnas.2022859118.

Hoose, C., and O. Möhler. 2012. Heterogeneous ice nucleation on atmospheric aerosols: A review of results from laboratory experiments. *Atmos. Chem. Phys.* 12 (20): 9817–54. doi: 10.5194/acp-12-9817-2012.

House, M. L., and C. S. Dutcher. 2023. Microfluidic platform for coupled studies of freezing behavior and final effloresced particle morphology in snomax® containing aqueous droplets. *Aerosol Sci. Technol.* 58 (4):427–39. doi: 10.1080/02786826.2023.2233574.

Isenrich, F. N., N. Shardt, M. Rösch, J. Nette, S. Stavrakis, C. Marcolli, Z. A. Kanji, A. J. Demello, and U. Lohmann. 2022. The microfluidic ice nuclei counter Zürich (Mincz): A platform for homogeneous and heterogeneous ice nucleation. *Atmos. Meas. Tech.* 15 (18):5367–81. doi: 10.5194/amt-15-5367-2022.

Jing, X., J. Yang, T. Li, J. Hu, C. He, Y. Yin, P. J. DeMott, Z. Wang, H. Jiang, and K. Chen. 2022. Pre-activation of ice nucleating particles in deposition nucleation mode: Evidence from measurement using a static vacuum water vapor diffusion chamber in xinjiang, china. *Geophys. Res. Lett.* 49 (15):e2022GL099468. doi: 10.1029/2022GL099468.

Kaufhold, S., R. Dohrmann, M. Klinkenberg, S. Siegesmund, and K. Ufer. 2010. N2-bet specific surface area of bentonites. *J. Colloid Interface Sci.* 349 (1):275–82. doi: 10.1016/j.jcis.2010.05.018.

Keene, W. C., R. Sander, A. A. P. Pszenny, R. Vogt, P. J. Crutzen, and J. N. Galloway. 1998. Aerosol ph in the marine boundary layer: A review and model evaluation. *J. Aerosol Sci.* 29 (3):339–56. doi: 10.1016/S0021-8502(97)10011-8.

Klinger, C., G. Feingold, and T. Yamaguchi. 2019. Cloud droplet growth in shallow cumulus clouds considering 1-d and 3-d thermal radiative effects. *Atmos. Chem. Phys.* 19 (9):6295–313. doi: 10.5194/acp-19-6295-2019.

Klumpp, K., C. Marcolli, A. Alonso-Hellweg, C. H. Dreimol, and T. Peter. 2023. Comparing the ice nucleation properties of the kaolin minerals kaolinite and halloysite. *Atmos. Chem. Phys.* 23 (2):1579–98. doi: 10.5194/acp-23-1579-2023.

Kumar, A., K. Klumpp, C. Barak, G. Rytwo, M. Plötze, T. Peter, and C. Marcolli. 2023. Ice nucleation by smectites: The role of the edges. *Atmos. Chem. Phys.* 23 (8):4881–902. doi: 10.5194/acp-23-4881-2023.

Kumar, A., C. Marcolli, and T. Peter. 2019. Ice nucleation activity of silicates and aluminosilicates in pure water and aqueous solutions—part 3: Aluminosilicates. *Atmos.*

Chem. Phys. 19 (9):6059–84. doi: 10.5194/acp-19-6059-2019.

Liu, Z., D. Sun, B. Jiang, L. Shen, P. Zhou, C. Gao, Z. Jin, X. Liu, L. Yang, and S. Tan. 2023. Continuous gradient temperature control of microfluidic chip based on thermoelectric cooler. *Appl. Therm. Eng.* 234:121277. doi: 10.1016/j.applthermaleng.2023.121277.

Marcolli, C. 2017. Pre-activation of aerosol particles by ice preserved in pores. *Atmos. Chem. Phys.* 17 (3):1595–622. doi: 10.5194/acp-17-1595-2017.

Matsuki, A., A. Schwarzenboeck, H. Venzac, P. Laj, S. Crumeyrolle, and L. Gomes. 2010. Cloud processing of mineral dust: Direct comparison of cloud residual and clear sky particles during amma aircraft campaign in summer 2006. *Atmos. Chem. Phys.* 10 (3):1057–69. doi: 10.5194/acp-10-1057-2010.

Nandy, L., and C. S. Dutcher. 2018. Phase behavior of ammonium sulfate with organic acid solutions in aqueous aerosol mimics using microfluidic traps. *J. Phys. Chem. B* 122 (13):3480–90. doi: 10.1021/acs.jpcb.7b10655.

Nicola, B. P., K. Bernardo-Gusmão, and A. J. Schwanke. 2021. Smectite clay nanoarchitectures: Rational design and applications. In *Handbook of nanomaterials and nanocomposites for energy and environmental applications*, 275–305. Cham: Springer International Publishing.

Perkins, R. J., M. G. Vazquez De Vasquez, E. E. Beasley, T. C. J. Hill, E. A. Stone, H. C. Allen, and P. J. Demott. 2020. Relating structure and ice nucleation of mixed surfactant systems relevant to sea spray aerosol. *J. Phys. Chem. A* 124 (42):8806–21. doi: 10.1021/acs.jpca.0c05849.

Pinti, V., C. Marcolli, B. Zobrist, C. R. Hoyle, and T. Peter. 2012. Ice nucleation efficiency of clay minerals in the immersion mode. *Atmos. Chem. Phys.* 12 (13):5859–78. doi: 10.5194/acp-12-5859-2012.

Proske, U., V. Bessenbacher, Z. Dedekind, U. Lohmann, and D. Neubauer. 2021. How frequent is natural cloud seeding from ice cloud layers ($< -35\,^{\circ}C$) over switzerland? *Atmos. Chem. Phys.* 21 (6):5195–216. doi: 10.5194/acp-21-5195-2021.

Pujala, R. K., and H. B. Bohidar. 2019. Slow dynamics and equilibrium gelation in fractionated montmorillonite nanoplatelet dispersions. *Colloid Polym. Sci.* 297 (7-8):1053–65. doi: 10.1007/s00396-019-04507-4.

Quinn, P. K., T. S. Bates, D. J. Coffman, J. E. Johnson, and L. M. Upchurch, NOAA PMEL 2023. Climate roles of non-sea salt sulfate and sea spray aerosol in the atmospheric marine boundary layer: Highlights of 40 years of PMEL research. *Oceanog* 36:168–74. doi: 10.5670/oceanog.2023.202.

Reicher, N., L. Segev, and Y. Rudich. 2018. The Weizmann supercooled droplets observation on a microarray (wisdom) and application for ambient dust. *Atmos. Meas. Tech.* 11 (1):233–48. doi: 10.5194/amt-11-233-2018.

Riemer, N., A. P. Ault, M. West, R. L. Craig, and J. H. Curtis. 2019. Aerosol mixing state: Measurements, modeling, and impacts. *Rev. Geophys.* 57 (2):187–249. doi: 10.1029/2018RG000615.

Roy, P., M. L. House, and C. S. Dutcher. 2021. A microfluidic device for automated high throughput detection of ice nucleation of snomax®. *Micromachines (Basel).* 12 (3):296. doi: 10.3390/mi12030296.

Roy, P., L. E. Mael, T. C. J. Hill, L. Mehndiratta, G. Peiker, M. L. House, P. J. Demott, V. H. Grassian, and C. S. Dutcher. 2021. Ice nucleating activity and residual particle morphology of bulk seawater and sea surface microlayer. *ACS Earth Space Chem.* 5 (8):1916–28. doi: 10.1021/acsearthspacechem.1c00175.

Schuster, G. L., B. Lin, and O. Dubovik. 2009. Remote sensing of aerosol water uptake. *Geophys. Res. Lett.* 36 (3):n/a–/a. doi: 10.1029/2008GL036576.

Segad, M., S. Hanski, U. Olsson, J. Ruokolainen, T. Åkesson, and B. Jönsson. 2012. Microstructural and swelling properties of ca and na montmorillonite: (in situ) observations with cryo-tem and saxs. *J. Phys. Chem. C* 116 (13):7596–601. doi: 10.1021/jp300531y.

Sihvonen, S. K., K. A. Murphy, N. M. Washton, M. B. Altaf, K. T. Mueller, and M. A. Freedman. 2018. Effect of acid on surface hydroxyl groups on kaolinite and montmorillonite. *Zeitschrift Für Physikalische Chemie* 232 (3):409–30. doi: 10.1515/zpch-2016-0958.

Sihvonen, S. K., G. P. Schill, N. A. Lyktey, D. P. Veghte, M. A. Tolbert, and M. A. Freedman. 2014. Chemical and physical transformations of aluminosilicate clay minerals due to acid treatment and consequences for heterogeneous ice nucleation. *J. Phys. Chem. A* 118 (38):8787–96. doi: 10.1021/jp504846g.

Suman, K., and Y. M. Joshi. 2018. Microstructure and soft glassy dynamics of an aqueous laponite dispersion. *Langmuir* 34 (44):13079–103. doi: 10.1021/acs.langmuir.8b01830.

Szakáll, M., M. Debertshäuser, C. P. Lackner, A. Mayer, O. Eppers, K. Diehl, A. Theis, S. K. Mitra, and S. Borrmann. 2021. Comparative study on immersion freezing utilizing single-droplet levitation methods. *Atmos. Chem. Phys.* 21 (5):3289–316. doi: 10.5194/acp-21-3289-2021.

Tarn, M. D., S. N. F. Sikora, G. C. E. Porter, J.-U. Shim, and B. J. Murray. 2021. Homogeneous freezing of water using microfluidics. *Micromachines (Basel).* 12 (2):223. doi: 10.3390/mi12020223.

Vali, G. 1971. Quantitative evaluation of experimental results the heterogeneous freezing nucleation of supercooled liquids. *J. Atmos. Sci.* 28 (3):402–9. doi: 10.1175/1520-0469(1971)028<0402:Qeoera>2.0.co;2.

Vergara-Temprado, J., A. K. Miltenberger, K. Furtado, D. P. Grosvenor, B. J. Shipway, A. A. Hill, J. M. Wilkinson, P. R. Field, B. J. Murray, and K. S. Carslaw. 2018. Strong control of southern ocean cloud reflectivity by ice-nucleating particles. *Proc. Natl. Acad. Sci. USA* 115 (11):2687–92. doi: 10.1073/pnas.1721627115.

Vuong, S. M., and S. L. Anna. 2012. Tuning bubbly structures in microchannels. *Biomicrofluidics* 6 (2):22004–2200418. doi: 10.1063/1.3693605.

Wagner, R., K. Höhler, W. Huang, A. Kiselev, O. Möhler, C. Mohr, A. Pajunoja, H. Saathoff, T. Schiebel, X. Shen, et al. 2017. Heterogeneous ice nucleation of α-pinene soa particles before and after ice cloud processing. *JGR. Atmos.* 122 (9):4924–43. doi: 10.1002/2016JD026401.

Wang, Z., T. Wang, H. Fu, L. Zhang, M. Tang, C. George, V. H. Grassian, and J. Chen. 2019. Enhanced heterogeneous uptake of sulfur dioxide on mineral particles through modification of iron speciation during simulated cloud processing. *Atmos. Chem. Phys.* 19 (19):12569–85. doi: 10.5194/acp-19-12569-2019.

Welti, A., F. Lüönd, O. Stetzer, and U. Lohmann. 2009. Influence of particle size on the ice nucleating ability of mineral dusts. *Atmos. Chem. Phys.* 9 (18):6705–15. doi: 10.5194/acp-9-6705-2009.

Wilkinson, N., A. Metaxas, E. Brichetto, S. Wickramaratne, T. M. Reineke, and C. S. Dutcher. 2017. Ionic strength dependence of aggregate size and morphology on polymer-clay flocculation. *Colloids Surf. A.* 529:1037–46. doi: 10.1016/j.colsurfa.2017.06.085.

Wilkinson, N., A. Metaxas, C. Quinney, S. Wickramaratne, T. M. Reineke, and C. S. Dutcher. 2018. Ph dependence of bentonite aggregate size and morphology on polymer-clay flocculation. *Colloids Surf. A.* 537:281–6. doi: 10.1016/j.colsurfa.2017.10.007.

Yao, Y., M. L. Dawson, D. Dabdub, and N. Riemer. 2021. Evaluating the impacts of cloud processing on resuspended aerosol particles after cloud evaporation using a particle-resolved model. *JGR. Atmos.* 126 (24). doi: 10.1029/2021JD034992.

Zimmermann, F., S. Weinbruch, L. Schütz, H. Hofmann, M. Ebert, K. Kandler, and A. Worringen. 2008. Ice nucleation properties of the most abundant mineral dust phases. *J. Geophys. Res.* 113 (D23). doi: 10.1029/2008JD010655.